Structure of quantum dots as seen by excitonic spectroscopy versus structural characterization: Using theory to close the loop

V. Mlinar,[1] M. Bozkurt,[2] J. M. Ulloa,[2] M. Ediger,[3] G. Bester,[4] A. Badolato,[5] P. M. Koenraad,[2]
R. J. Warburton,[3] and A. Zunger[1]
[1]*National Renewable Energy Laboratory, Golden, Colorado 80401, USA*
[2]*Department of Applied Physics, Eindhoven University of Technology, P.O. Box 513, NL-5600MB Eindhoven, The Netherlands*
[3]*School of Engineering and Physical Sciences, Heriot-Watt University, Edinburgh EH14 4AS, United Kingdom*
[4]*Max Planck Institute for Solid State Research, Heisenbergstrasse 1, 70569 Stuttgart, Germany*
[5]*Department of Physics and Astronomy, University of Rochester, Rochester, New York 14627, USA*
(Received 4 September 2009; published 23 October 2009)

Structure-spectra relationship in semiconductor quantum dots (QDs) is investigated by subjecting the same QD sample to single-dot spectroscopy and cross-sectional scanning tunneling microscopy (XSTM) structural measurements. We find that the conventional approach of using XSTM structure as input to calculate the spectra produces some notable conflicts with the measured spectra. We demonstrate a theoretical "inverse approach" which deciphers structural information from the measured spectra and finds structural models that agree with both XSTM and spectroscopy data. This effectively "closes the loop" between structure and spectroscopy in QDs.

DOI: 10.1103/PhysRevB.80.165425 PACS number(s): 73.21.La, 02.30.Zz, 68.65.−k, 78.67.−n

I. INTRODUCTION

At the heart of structural chemistry and molecular spectroscopy lies the premise that spectra reflect structure and thus that the understanding of the spectra is greatly facilitated by the knowledge of the structure and symmetry.[1] Although the structure can be readily measured in discrete molecules or crystalline compounds, this is more problematic for nanostructures and microstructures that emerge as precipitates from a matrix.[2–4] Examples include colloidal nanocrystals which are precipitated out of a solution containing organometallic surfactants,[2] quantum wires precipitated from liquid semiconductor in the presence of metal catalysts,[3] and "self-assembled" semiconductor quantum dots (QDs) emerging from a lattice-mismatched matrix on which the QDs are grown epitaxially.[4] Such highly useful objects contain a few hundred to a few million atoms, can exist in a quasicontinuous range of compositions, possibly with a composition gradient within the structure, and come in a variety of shapes and sizes.[2–4] The complexity of such structures has generally prohibited atomic-scale experimental characterization or theoretical prediction of their structure. Indeed, only the global features—the size, shape, and composition (which we refer to as "SSC"), are generally assessed.[5] Furthermore, the accuracy of such features may depend critically on the models used to analyze the data.[5] Yet, in the theory of quantum nanostructures,[6–10] one calculates spectra based on the assumed SSC, and compares it with the measured spectrum. It is, however, not clear to what extent the currently assumed SSCs (Ref. 5) reflect the "real structure" and whether the assumed SSCs can be used to predict the spectra. The present paper addresses this central structural deficiency problem.

QDs can be grown deterministically and reproducibly by established synthesis protocols that afford significant control over the outcome;[4,6] they can be characterized with both cross-sectional scanning tunneling microscopy (XSTM) (Refs. 11–13) and optical spectroscopy, for instance multiexciton photoluminescence (PL).[6,7,14] Despite this, the atomic structure is unknown, so there is no structural basis for understanding the detailed and rich spectroscopy. Building such a bridge, linking XSTM and spectroscopic data on the same QD sample with an atomistic theory is challenging and is currently lacking for QDs. We indicate here how such a bridge between growth-structure-spectroscopy can be built.

XSTM has emerged as one of the leading structural characterization methods for individual nanostructures.[5,11–13] Unlike crystalline solids, where refinement of x-ray diffraction experiments tends to produce a rather unique, narrowly defined crystal structure whose description is mostly independent of the input guess,[15] XSTM is different in two principal ways. First, deducing the composition profile requires first guess of the shape of the QD—the "usual suspects" are the ones with high symmetry such as truncated pyramids, cones, and ellipsoids. The final shape and composition profile are selected from such a set of guessed inputs by fitting the measured outward relation of the QD on the cleaved surface.[11,13] Thus, a single XSTM measurement often produces a few final SSC models, all consistent with the same measured QD relaxation profile. Second, given that the application of the XSTM procedure to million-atom QDs reveals, in the final analysis, only global structural features, i.e., SSCs, one wonders to what extent is this restricted/specific structural information sufficient to determine other physical properties, such as detailed spectra.

Optically addressing individual QDs gives not only the energy of the fundamental exciton but also the shifts, typically a few meV, due to interdot Coulomb interactions on charging the QD with excess electrons or on creation of the biexciton. These various excitons have been identified unambiguously in the emission spectra of individual QDs,[18] but a connection between the energy shifts and the structure determined by XSTM has not been made previously.

Atomistic electronic structure theory of QDs (Refs. 16 and 17) can predict the detailed spectroscopic features given the discrete atomic-scale structure as input. Indeed, the many-body pseudopotential approach has emerged as a reliable method for describing various excitonic complexes.[6,9,18] To address the fundamental question raised above, we use here such a theoretical tool to bridge the structural (XSTM) and spectroscopic (PL) information. Specifically, we subject the same QD sample, produced by a well-defined growth protocol, both to spectroscopic and to XSTM measurements. Then, we use these different models, one at a time, as input to electronic structure theory and predict the corresponding multiexcitonic spectra. A comparison between the measured and calculated spectra is used to determine the appropriateness of the XSTM SSC profile to gauge spectroscopic features.

We find that the conventional approach of using XSTM structure as input to calculate the spectra creates some notable conflicts with the measured spectra. However, we demonstrate the "inverse approach" which deciphers structural information from the measured excitonic spectra and identifies structural models that agree with both XSTM and spectroscopic data. Unlike the commonly used approach, our inverse approach effectively "closes the loop" between the structure and spectra. We suggest that deciphering structural information from the optical spectra of large nanosystems in general should be used whenever the complexity of structure prohibits experimental characterization of the full, atomistic structure of the morphology.

II. CHARACTERIZATION OF QUANTUM DOTS

A. XSTM measurements give the height and base, but can yield many equally probable descriptions of the shape and composition profile

The QDs studied here were (In,Ga)As, grown by MBE on (100) GaAs substrate (see Appendix).[6] The sample was cleaved at the perpendicular (110) surface enabling STM with atomic resolution to image the cross-sectional surface through the QDs.[11,13] The XSTM results are from one of the QDs presenting the largest cross-section.[11,13] The bias applied to the sample was −2.8 V and under these circumstances, electrons tunnel from the sample to the tip from the occupied valence-band/QD hole states and the total current is mainly sensitive to topographic profiles of the sample surface and to a much smaller extent sensitive to the electronic contrast (offset GaAs valence band and QD hole state).[13] From the recorded topographic image the base-length (b_{geom}) and height (h_{geom}) of the QD are extracted; in our case 24 and 7 nm, respectively, as shown in Fig. 1(a). However, the shape and composition profile of the QD remain unknown.[13] To analyze this, one measures the relaxation of the cleaved surface [Fig. 1(b)] and compares it with the calculated relaxation profile, fitting a shape and composition profile of the QD. The quality of the fit is judged by the root-mean-square (RMS) deviations. Figure 1(c) shows a variety of shapes and profiles that all agree with the measured relaxation profile [see Fig. 1(b)]. We next examine their ability to explain the spectra.

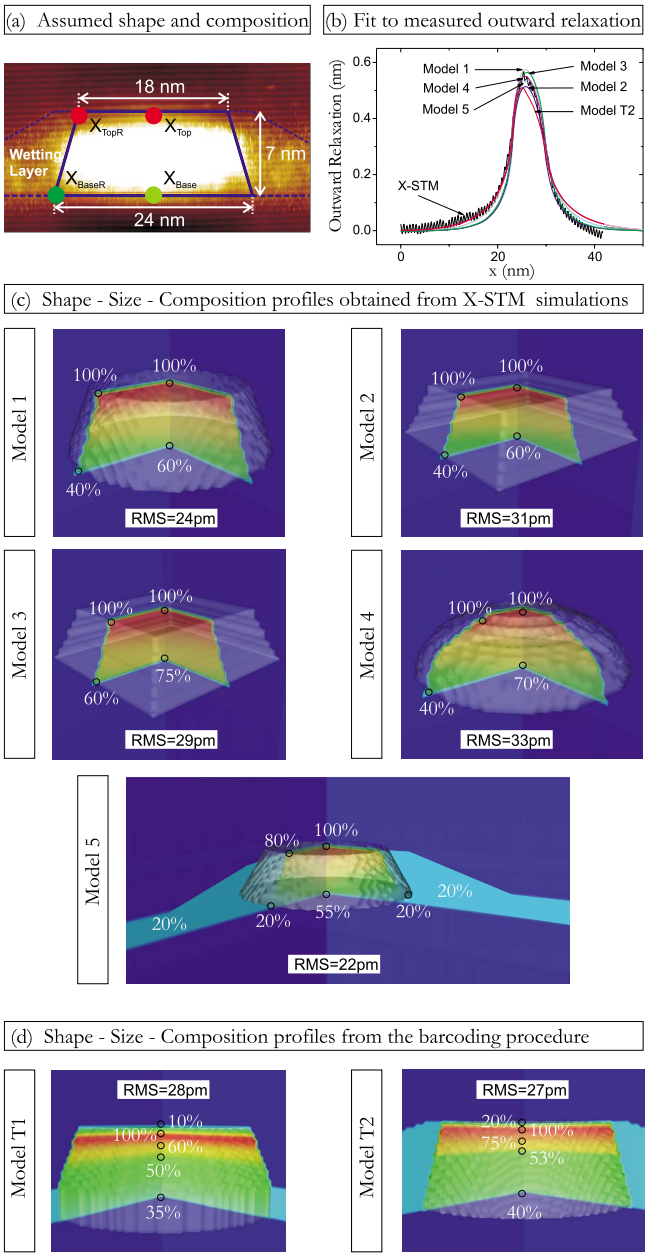

FIG. 1. (Color online) Extraction of SSC profiles by XSTM measurements and modeling. (a) A shape of model QD using base length and height extracted from XSTM measurements. The composition profile $C_{In}(x,y,z)$ is constructed by fitting In composition at four points $(X_{Base}, X_{BaseR}, X_{Top}, X_{TopR})$, $C_{In}(x,y,z) = X_0 + [(x/b_{geom})^2 + (y/b_{geom})^2]^{1/2}(X_R - X_0)$, where $X_0 = X_{Base} + (X_{Top} - X_{Base})(z/h_{geom})$, $X_R = X_{BaseR} + (X_{TopR} - X_{BaseR})(z/h_{geom})$. (b) Measured outward relaxation curve (black) is fitted by a few models that vary the composition profile for a given shape using continuum elasticity simulation. This produces (c) model SSC profiles of five model QDs. Indium composition profile is shown by contour plot where 20% of In is represented by cyan (light gray) color, 40% of In concentration by green (gray), and 100% by red (dark gray). (d) Spectroscopically deduced model QDs via the barcoding approach (Ref. 21). In parts (c) and (d) the error of the calculated relaxation profile relative to measured relaxation (b) is judged by the RMS deviations.

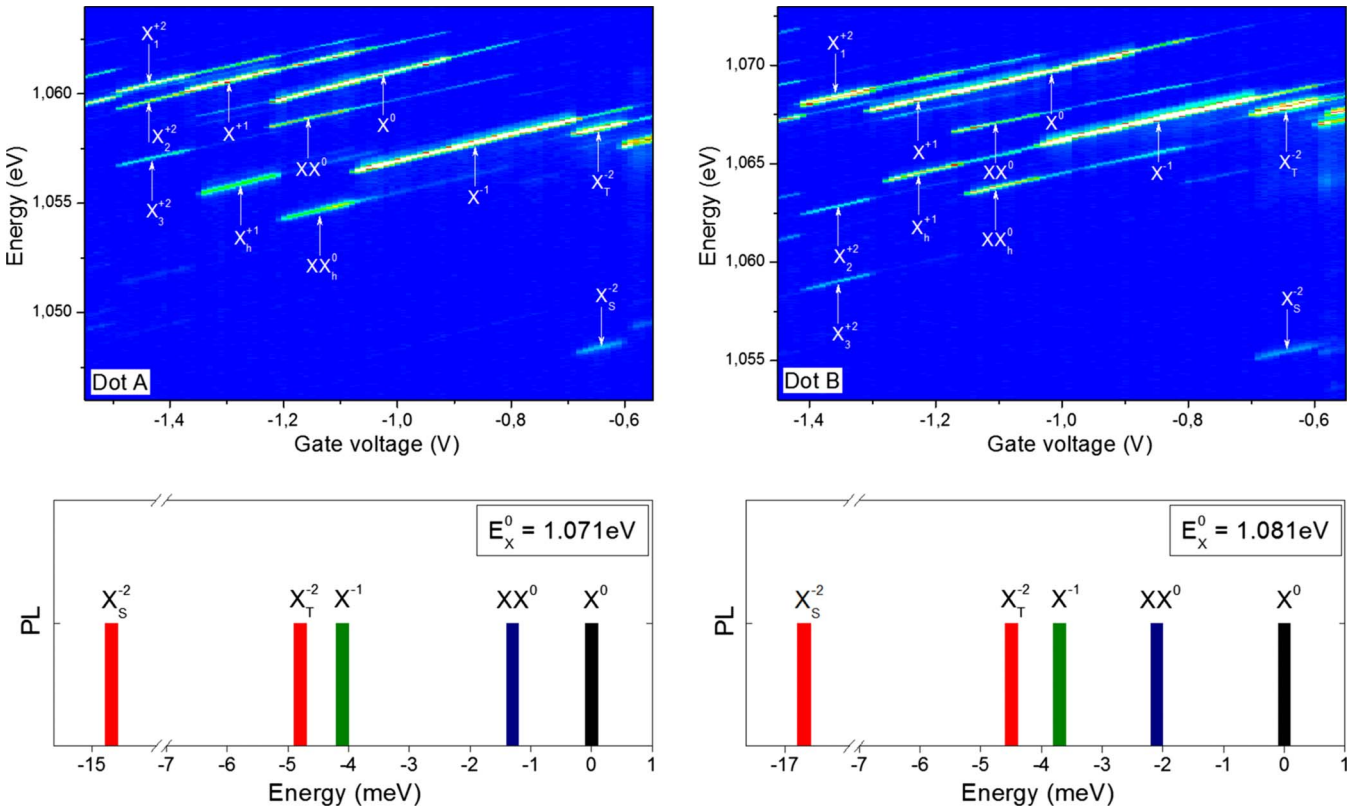

FIG. 2. (Color online) Measured and assigned photoluminescence energy vs gate voltage (upper panel) from which a multiexciton sequence (bottom panel) is extracted for two prototype QDs emitting around ~1 eV. Multiexcitonic transition energies are given relative to monoexciton energy (for QD A E_X^0=1.071 eV, and for QD B E_X^0=1.081 eV).

B. Single-dot spectroscopy

Figure 2 shows the measured multiexcitonic PL spectra (see Appendix) of two typical QDs from the *same* sample of QDs, showing exciton energies in the range of 1.07–1.08 eV. The labels refer to different excitons: monoexciton (X^0) has one electron and one hole; the negative trion (X^{-1}) has two electrons and one hole; the doubly-negative monoexciton (X^{-2}) has three electrons and one hole (giving rise to two lines, "triplet" X_T^{-2} and "singlet" X_S^{-2} emission); and the neutral biexciton (XX^0) has two electrons and two holes. There are of course QD-to-QD variations in the emission spectra [Fig. 2 top]. However, the sequence of X^0, XX^0, X^{-1}, and X^{-2} emission lines in the measured PL spectra from each and every QD studied in the ensemble produced by this well-established growth protocol is kept. This can be broken down into three "hard rules" (HRs). Hard rule 1, HR1: the energies of X^{-1}, XX^0, and X^{-2} emission lines are always red shifted relative to X^0. HR2: XX^0 always lies between X^0 and X^{-1}. HR3: X_T^{-2} is always redshifted relative to X^{-1}.

III. STRUCTURE-SPECTRA RELATIONSHIP

A. Conventional approach: XSTM structural determination→theory of spectra→measured spectra produces inconsistencies

Each of the five XSTM deduced models SSCs [Fig. 1(c)] is next used as an input to the many-body pseudopotential calculations to predict the multiexcitonic spectra. We use a theoretical approach (see Appendix) that includes the relevant single-body (band mixing, intervalley mixing) and all types of many-body interactions (direct, exchange and correlation).[16,17] Our theory of QDs can predict the detailed spectroscopic features given the discrete atomic-scale structure as input and has emerged as a reliable method for describing various excitonic complexes.[6,18] Fig. 3 shows calculated multiexcitonic spectra of the XSTM model QDs using the XSTM structures as input. Given that each XSTM deduced model QDs is a representative of the ensemble of QDs,[19] when comparing to the measured spectra, we set the requirements that the calculated spectrum of each XSTM model QD (i) has exciton energy (E_X^0) close to the experimental values and (ii) three hard rules are satisfied. Thus, we discuss only the hard rules which are common to the spectra from all QDs in the sample, but not the distances between the emission peaks or intensities of peaks in the spectra as they vary from QD-to-QD throughout the sample.[19]

The calculated E_X^0 energies of all five XSTM model QDs in Fig. 3 are in a good agreement with the measured E_X^0 energies. Thus, the XSTM procedure provides a good estimate of the overall QD geometry and average composition profile, which together determine the E_X^0 energy. Moving to the high-resolution spectroscopic information, we find that all five models extracted from XSTM fail to reproduce the universal sequence of lines (hard rules) observed in PL.[20] This disconnect between spectroscopy and structural charac-

terization may suggest that the structural features responsible for the "spectroscopic hard rules" are missing from current XSTM deduced SSC models. The consequence is that the XSTM→theory→spectroscopy route does not "close the loop." We note that in a similar way, XSTM was previously used to determine the interfacial profiles in (In,Ga)As/InP quantum-wells,[22] where many XSTM structural models fit equally well the measured outward relaxation, but most did not reproduce the measured X^0 peak.

B. Inverse approach: decipher structural information from the measured spectra

Since the XSTM structure→theory of spectra →measured spectra fails, we will use an inverse approach, determining at the outset those structural motifs "seen" by the spectra—spectroscopic SSC. We will let the spectra narrow down the space of SSC configurations that have no conflict with the hard rules. In doing so we take two key steps:

First, the spectral "barcoding" procedure[21] we use involves the calculation of the multiexcitonic spectra of a library of 200–300 assumed QD structures. Then, we use data reduction technique to distill from the library the links between structural motifs and particular sequences ("barcodes") of excitonic lines. Once this is done we can inquire which structural motifs are responsible for satisfying the observed HRs. We find three structural motifs [QD base-length (b_{Spectr}), height (h_{Spectr}), and average In composition ($\bar{C}_{In}$)] that control the spectroscopic HRs, whereas the remaining structural motifs [e.g., QD shape, or composition profile] do not influence this sequence. Figure 4(a) illustrates the variation in the sequence of multiexcitonic transitions, with the h_{Spectr} and b_{Spectr}, for $\bar{C}_{In} \geq 80\%$. We can identify four regions ("phases"), associated with critical spectroscopic heights h_1-h_3, that depend on average In composition $h_i = f(\bar{C}_{In})$, $i = 1,2,3$. In Region I ($h_{Spectr} < h_1$), all three HRs are satisfied (for example, we calculate $h_1 = 3.5$ nm for $\bar{C}_{In} = 80\%$). In region II, where $h_1 < h_{Spectr} < h_2$, HR2 is violated, i.e., X^{-1} (and X_T^{-2}) emission line is blueshifted relative to XX^0. In region III, where $h_2 < h_{Spectr} < h_3$, HR1 and HR2 are both violated because of the blueshifted X^{-1} and X_T^{-2} emission lines relative to X^0, but XX^0 remains redshifted. The XSTM model 5 belongs to this region. In region IV, where $h_3 < h_{Spectr}$, all HRs are violated because all emission lines are blueshifted relative to X^0. The XSTM deduced model 1–4 QDs belong to this region. We see that all XSTM models are rather far from region I that gives the correct sequence X^0, XX^0, X^{-1}, and X^{-2} of the multiexciton lines. XSTM measurements provide, with high accuracy, geometric size of the QD, but the In composition gradient is accessed only indirectly through the measured outward relaxation (whose degree of correlation with the composition profile is unknown). However, it is the In composition gradient $C_{In}(x,y,z)$, that within measured geometric size determines the QD spectroscopic size (i.e., QD size "seen" by the spectroscopy).

Second, we will use the spectral barcoding procedure to deduce composition profile within geometric QD size. Indium composition gradient determines (through a combination of compositions and strain) the wave function quantum confinement, i.e., spectroscopic size, in lateral direction—spectroscopic base length, and in growth direction—spectroscopic height. We fix the QD shape to a truncated cone[23] and vary the In gradient so that the spectroscopic size of the QD belongs to region I in the phase diagram of Fig. 4(a). Furthermore, the average In composition ($\bar{C}_{In}$) within this spectroscopic SSC has to yield an exciton energy $E_X^0 = 1.088 \pm 0.025$ eV. This establishes the range of SSCs which a QD has to maintain to satisfy HRs. Given the range of exciton energies the spectroscopic SSC of QD is given by: $\bar{C}_{In} = 85 \pm 5\%$, $b_{Spectr} = 20 \pm 2$ nm, and h_{Spectr}

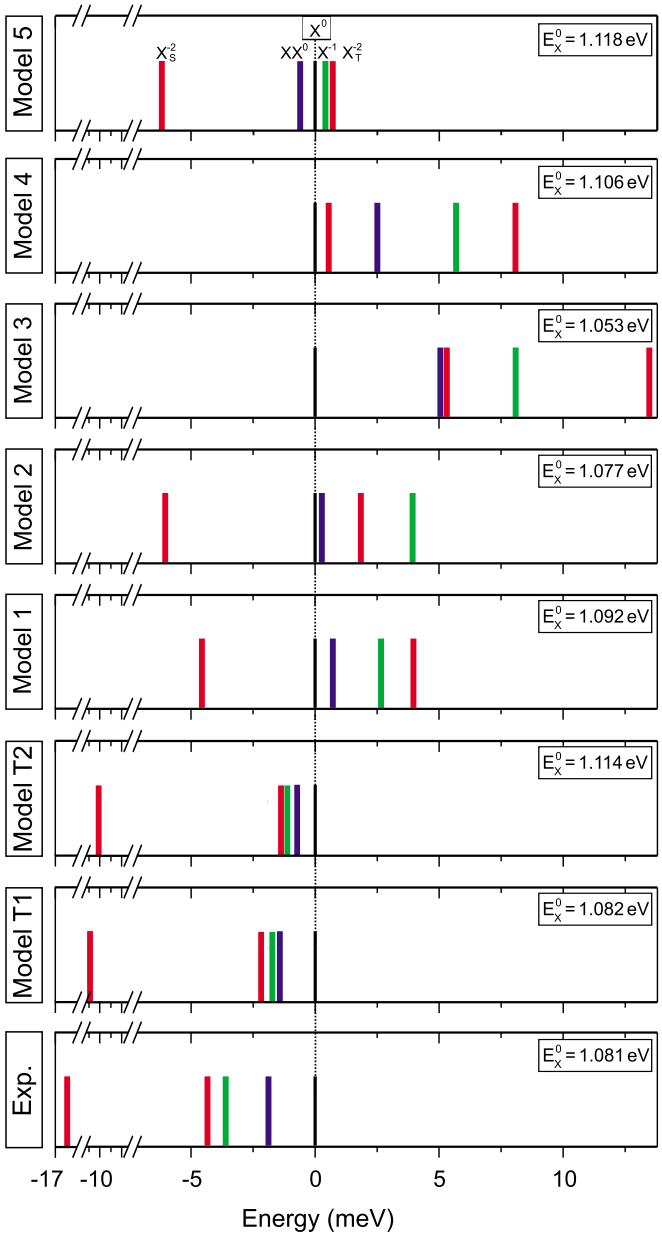

FIG. 3. (Color online) Calculated emission spectra for exciton charges X^0, XX^0, X^{-1}, and X^{-2} of the XSTM deduced models 1–5 QDs [shown in Fig. 2(c)]. QDs T1 and T2 are spectroscopically deduced via the barcoding procedure (Ref. 21). These are compared with experiment.

$=2.5\pm0.38$ nm. We generate two such model QDs. The SSCs of these QDs, denoted as models T1 and T2, are shown in Fig. 1(d).

The calculated spectra of model T1 and T2 are shown in Fig. 3 and are compared with spectroscopy. Subjecting these spectroscopically deduced QDs to a calculation of outward relaxation [Fig. 1(b)] shows that the models T1 and T2 fit the XSTM measured outward relaxation within RMS=28 pm, comparable to all XSTM models. Thus, the spectroscopy (plus geometric size)→Theory→XSTM route successfully "closes the loop," producing a structural description of the QD compatible *with two independent experimental data*: structural (XSTM) and spectroscopic (PL) data. Note that in order to reproduce the measured spectral HRs and $E_X^0=1.088\pm0.025$ eV, only spectroscopic base-length (b_{Spectr}), spectroscopic height (h_{Spectr}), and average indium composition [$\bar{C}_{In}\geq80\%$] are needed [Region I in Fig. 4(a)]. QD shape, geometrical base-length (b_{geom}), and geometrical height (h_{geom}) [Fig. 1(a)] are not deduced by the inverse procedure, but from the XSTM measurements, so that the structural model QD matches XSTM data too. Variation in QD shape [e.g., from a truncated cone to cylinder] would not influence agreement with the spectroscopic HRs [see Ref. 21], but would present variance with XSTM outward relaxation.

IV. STRUCTURAL PROPERTIES OF SPECTROSCOPICALLY DEDUCED QUANTUM DOTS

A. Spectroscopically determined composition profile

Figure 4(b) shows the spectroscopically deduced in profile and compares it to the linear In profile of the model 5 QD. The inverse approach presented here shows that the QD structure which matches both the outward relaxation of XSTM measurements and the measured spectra reveals a nonlinear, almost abrupt, variation in composition profile in the growth direction [Fig. 1(d)]. In the absence of other information, a linear variation in In composition in the growth direction has been previously assumed in literature,[24,11–13] however not without conflicts.[25,26] The emergence of an abrupt In composition profile from our analysis of the spectroscopy finds independent support from transmission electron microscopy dark images of In-low (In,Ga)As QDs,[25] and from a developed structural characterization technique coherent Bragg rod analysis[26] that showed dramatically nonlinear composition profiles for InGaAsSb QDs. Furthermore,

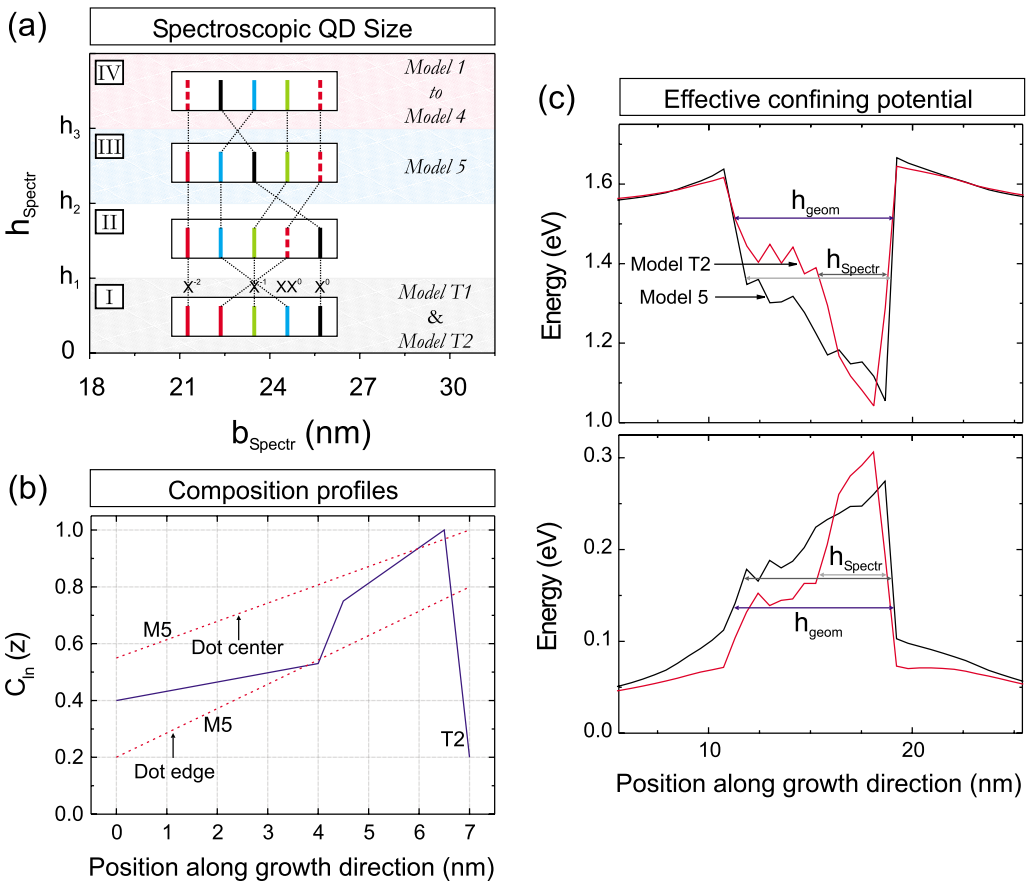

FIG. 4. (Color online) (a) Phase diagram of sequence of emission lines as a function of QD height (h_{Spectr}) and spectroscopic base-length (b_{Spectr}) for average In composition $\bar{C}_{In}\geq80\%$. $h_i=f(\bar{C}_{In})$, where $i=1,2,3$. For example for $\bar{C}_{In}=80\%$, $h_1=3.5$ nm, $h_2=4.5$ nm, and $h_3=5.5$ nm. Regions I–IV represent different type of line sequences. Only region I satisfies spectral HRs. (b) $C_{In}(z)$ in the growth direction of model 5 (red dotted lines) and model T2 (blue solid curve). (c) Calculated effective confining potential for electrons and holes obtained for model 5 (black) and model T2 (red) QDs. In the QD region the offsets are irregular (jagged) due to alloy fluctuations. Atomic-scale alloy randomness (Ref. 28) presents slight variations of effective confining potential, but does not influence the spectral HRs (Ref. 21).

our calculated wave functions for the model T1 and T2 are localized close to the top of the QD. Similar was observed for the measured wave functions of Ref. 27.

B. Geometric size versus spectroscopic size

Figure 4(c) shows the calculated (strain-and-composition-gradient modified) confining potential for electrons and holes obtained for a QD with the dimensions extracted from XSTM measurements ("geometric dimensions"), but having a linear composition profile (model 5). It is compared with a QD with an nonlinear composition profile (model T2). We see that the nonlinear In profile has a much narrower region of confinement (horizontal arrows) than the QD with linear In profile (Model 5) even though both have identical geometric sizes. For example, a QD with geometric height of 7 nm that starts with 40% In at its bottom and evolves, through some nonlinear (rather abrupt) composition gradient, to 100% In at its top, can have an effective "spectroscopic height" much less than 7 nm. Clearly, the effective spectroscopic height can be significantly different than the geometric height. This conclusion was also suggested in Ref. 11.

V. SUMMARY

We find that the inverse approach: spectroscopy (plus geometric size) $\rightarrow$ theory $\rightarrow$ XSTM, and not the conventional approach: XSTM $\rightarrow$ Theory $\rightarrow$ Spectroscopy, successfully "closes the loop" between the structure and spectra in QDs. We find the measured excitonic spectra encode structural information which combined with the geometric size from XSTM enables us to determine the main structural motifs of a QD. Such spectroscopically deduced QDs are compatible with both structural (XSTM) and spectroscopic (PL) data. We emphasize that research of spectroscopy-controlling structural features can be the key to design of nanostructures with target optical properties.

ACKNOWLEDGMENTS

Work at NREL was funded by the U. S. Department of Energy, Office of Science, under NREL contract No. DE-AC36-08GO28308. Work in UK was funded by EPSRC.

APPENDIX: METHODS

Growth protocol of QDs: the InAs QDs studied here are grown by molecular beam epitaxy on a (100) semi-insulating GaAs substrate. The QD layer is separated by 17 nm of intrinsic GaAs from a Si-doped n^{++} GaAs layer. QDs are capped with 10 nm of undoped GaAs followed by a 105 nm AlAs/GaAs superlattices. Samples used for XSTM and optical spectroscopy were adjacent parts of the same wafer.

Optical Spectroscopy: a charge-tunable device is made out of a 5 mm $\times$ 5 mm piece of wafer material. Ohmic contacts are prepared to the back contact, the earth, after which a 5-nm-thick NiCr Schottky barrier is evaporated onto the sample surface.[6] PL experiments on single QDs are carried out at 4.2 K using nonresonant excitation of the wetting layer. The emission is detected with an InGaAs array detector. There is clear single electron charging as a function of bias applied to the top gate allowing an unambiguous determination of the PL lines. The exciton lines exhibit a Stark shift but the energy differences between the exciton lines have at most a small dependence on bias. The Stark shift does not change the ordering of the exciton lines shown in the experimental barcodes in Fig. 2.

Pseudopotential many-body calculations: we accept as input the shape-size-composition profile of a QD, then relax the atomic position $\{\mathbf{R}_{i,\alpha}\}$ via valence force field method, and then construct the total pseudopotential of the system $V(\mathbf{r})$ by superposing the atomic pseudopotential $v_\alpha(\mathbf{r})$ centered at the atomic equilibrium positions for 2×10^6 atoms. We add the nonlocal spin-orbit V_{so} interaction, to yield the total potential $V(\mathbf{r})=V_{so}+\Sigma v_\alpha(\mathbf{r}-\mathbf{R}_{i,\alpha})$. The Hamiltonian $-1/2\nabla^2+V(\mathbf{r})$ is diagonalized in a basis $\{\phi_{n,\epsilon,\lambda}(\mathbf{k})\}$ of Bloch bands, of band index n and wave-vector k, for material λ (InAs, GaAs).[16] Multiexciton complexes are extracted from the configuration interaction (CI) method which takes into account direct Coulomb interaction, exchange, and correlations.[17] Coulomb and exchange integrals are computed numerically from the pseudopotential single-particle states using the microscopic dielectric constant. We checked the convergence of the CI by increasing the initial number of basis states, 12 electron and 12 hole single-particle states (counting spin) to 20 electron and 20 hole single-particle states and found no change in order of emission lines.

[1] G. M. Barrow, *Introduction to Molecular Spectroscopy* (McGraw-Hill, New York, 1962).
[2] A. P. Alivisatos, Science **271**, 933 (1996).
[3] J. Hu, M. Ouyang, P. Yang, and C. M. Lieber, Nature (London) **399**, 48 (1999).
[4] V. Shchukin, N. N. Ledentsov, and D. Bimberg, *Epitaxy of Nanostructures, Nanoscience and Technology* (Springer, New York, 2003).
[5] J. Stangl, V. Holý, and G. Bauer, Rev. Mod. Phys. **76**, 725 (2004).
[6] M. Ediger, G. Bester, A. Badolato, P. M. Petroff, K. Karrai, A. Zunger, and R. J. Warburton, Nat. Phys. **3**, 774 (2007).
[7] S. Rodt, A. Schliwa, K. Pötschke, F. Guffarth, and D. Bimberg, Phys. Rev. B **71**, 155325 (2005).
[8] P. Kratzer, Q. K. K. Liu, P. Acosta-Diaz, C. Manzano, G. Costantini, R. Songmuang, A. Rastelli, O. G. Schmidt, and K. Kern, Phys. Rev. B **73**, 205347 (2006).
[9] V. Mlinar, A. Franceschetti, and A. Zunger, Phys. Rev. B **79**, 121307(R) (2009).
[10] B. Szafran, Phys. Rev. B **77**, 205313 (2008).
[11] J. H. Blokland, M. Bozkurt, J. M. Ulloa, D. Reuter, P. M. Koenraad, P. C. M. Christianen, and J. C. Maan, Appl. Phys. Lett. **94**, 023107 (2009).
[12] N. Liu, J. Tersoff, O. Baklenov, Jr., A. L. Holmes, and C. K.

Shih, Phys. Rev. Lett. **84**, 334 (2000).
[13] M. Bruls, J. W. A. M. Vugs, P. M. Koenraad, H. W. M. Salemnik, J. H. Wolter, M. Hopkinson, M. S. Skolnick, F. Long, and S. P. A. Gill, Appl. Phys. Lett. **81**, 1708 (2002).
[14] P. A. Dalgarno, J. M. Smith, J. McFarlane, B. D. Gerardot, K. Karrai, A. Badolato, P. M. Petroff, and R. J. Warburton, Phys. Rev. B **77**, 245311 (2008).
[15] H. M. Rietveld, J. Appl. Crystallogr. **2**, 65 (1969).
[16] L.-W. Wang and A. Zunger, Phys. Rev. B **59**, 15806 (1999).
[17] A. Franceschetti, H. Fu, L.-W. Wang, and A. Zunger, Phys. Rev. B **60**, 1819 (1999).
[18] M. Ediger, G. Bester, B. D. Gerardot, A. Badolato, P. M. Petroff, K. Karrai, A. Zunger, and R. J. Warburton, Phys. Rev. Lett. **98**, 036808 (2007).
[19] In the XSTM procedure, one assumes uniform QD size and shape distribution over the sample (Refs. 11 and 13), and based on that assumption extracts the QD geometric size and deduces QD shape and composition. Thus, a XSTM deduced SSC [Fig. 1(c)] is rather a representative of the ensamble than a SSC of an individual QD.
[20] Error bars on the XSTM height are around 10–15%. This means that the error bar in the outward relaxation curves is 1/10-th–1/7-th of the measured outward relaxation. Including this uncertainty in the calculations does not allow us to reproduce the spectroscopic HRs.
[21] V. Mlinar and A. Zunger, Phys. Rev. B **80**, 035328 (2009).
[22] H. Chen, H. A. McKay, R. M. Feenstra, G. C. Aers, P. J. Poole, R. L. Williams, S. Charbonneau, P. G. Piva, T. W. Simpson, and I. V. Mitchell, J. Appl. Phys. **89**, 4815 (2001).
[23] The truncated cone was the best candidate to account for the outward relaxation [models 1 and 5 QDs in Fig. 1(c)] and also when considering the outward relaxation at different positions through the QD (Ref. 11).
[24] P. W. Fry, I. E. Itskevich, D. J. Mowbray, M. S. Skolnick, J. J. Finley, J. A. Barker, E. P. O'Reilly, L. R. Wilson, I. A. Larkin, P. A. Maksym, M. Hopkinson, M. Al-Khafaji, J. P. R. David, A. G. Cullis, G. Hill, and J. C. Clark, Phys. Rev. Lett. **84**, 733 (2000).
[25] A. Lemaître, G. Patriarche, and F. Glass, Appl. Phys. Lett. **85**, 3717 (2004).
[26] D. P. Kumah, S. Shusterman, Y. Paltiel, Y. Yacoby, and R. Clarke, Nat. Nanotechnol. (to be published).
[27] A. Urbieta, B. Grandidier, J. P. Nys, D. Deresmes, D. Stiévenard, A. Lemaître, G. Patriarche, and Y. M. Niquet, Phys. Rev. B **77**, 155313 (2008).
[28] V. Mlinar and A. Zunger, Phys. Rev. B **79**, 115416 (2009).